

## Electronic Supplementary Information for “Influence of polyelectrolyte shape on its sedimentation behavior: effect of relaxation electric field”

Pin-Hua Yeh,<sup>1</sup> Jyh-Ping Hsu,<sup>1,\*</sup> Shiojenn Tseng<sup>2,\*</sup>

<sup>1</sup>Department of Chemical Engineering, National Taiwan University, Taipei, Taiwan  
10617 Tel: 886-2-23637448, Fax: 886-2-23623040, E-mail: jphsu@ntu.edu.tw

<sup>2</sup>Department of Mathematics, Tamkang University, Tamsui, Taipei, Taiwan 25137, E-mail: topology@mail.tku.edu.tw

\* Corresponding author

### S1. Model verification by analytical and numerical results

To verify the applicability of the present model and the software adopted, the settling of an isolated rigid spherical TiO<sub>2</sub> particle of radius  $3 \times 10^{-7}$  m, scaled zeta potential  $\hat{\zeta} = 3$ , and density  $\rho_p = 4000$  kg/m<sup>3</sup> in an aqueous KCl solution subject to a gravitational or centrifugal field solved numerically by Keller et al.<sup>1</sup> is reanalyzed. Fig. S1 summarizes their results for the scaled electric force ( $F_e/F_{e,\text{ref}}$ ), ( $F_e/F_h$ ), ( $F_e/F_{\text{Stokes}}$ ), and  $|\hat{U}_B|$ , and the corresponding results of our model. Here,  $F_{e,\text{ref}} = \varepsilon \phi_{\text{ref}}^2$ , is a reference electric force, ( $F_e/F_h$ ) the ratio of the electric force over the hydrodynamic force, ( $F_h/F_{\text{Stokes}}$ ) the scaled hydrodynamic force, and  $|\hat{U}_B|$  the magnitude of the scaled velocity.  $F_{\text{Stokes}} = 6\pi\eta a u_{\text{ref}}$  is a reference hydrodynamic force, the force acting on an isolated, rigid, uncharged sphere settling at Stokes velocity. Fig. S1 reveals that, in general, our results agree pretty well

with those of Keller et al.<sup>1</sup> Some deviation is observed in Fig. S1(b) for the scaled hydrodynamic force ( $F_h/F_{Stokes}$ ), but the percentage deviation is smaller than 3 %.

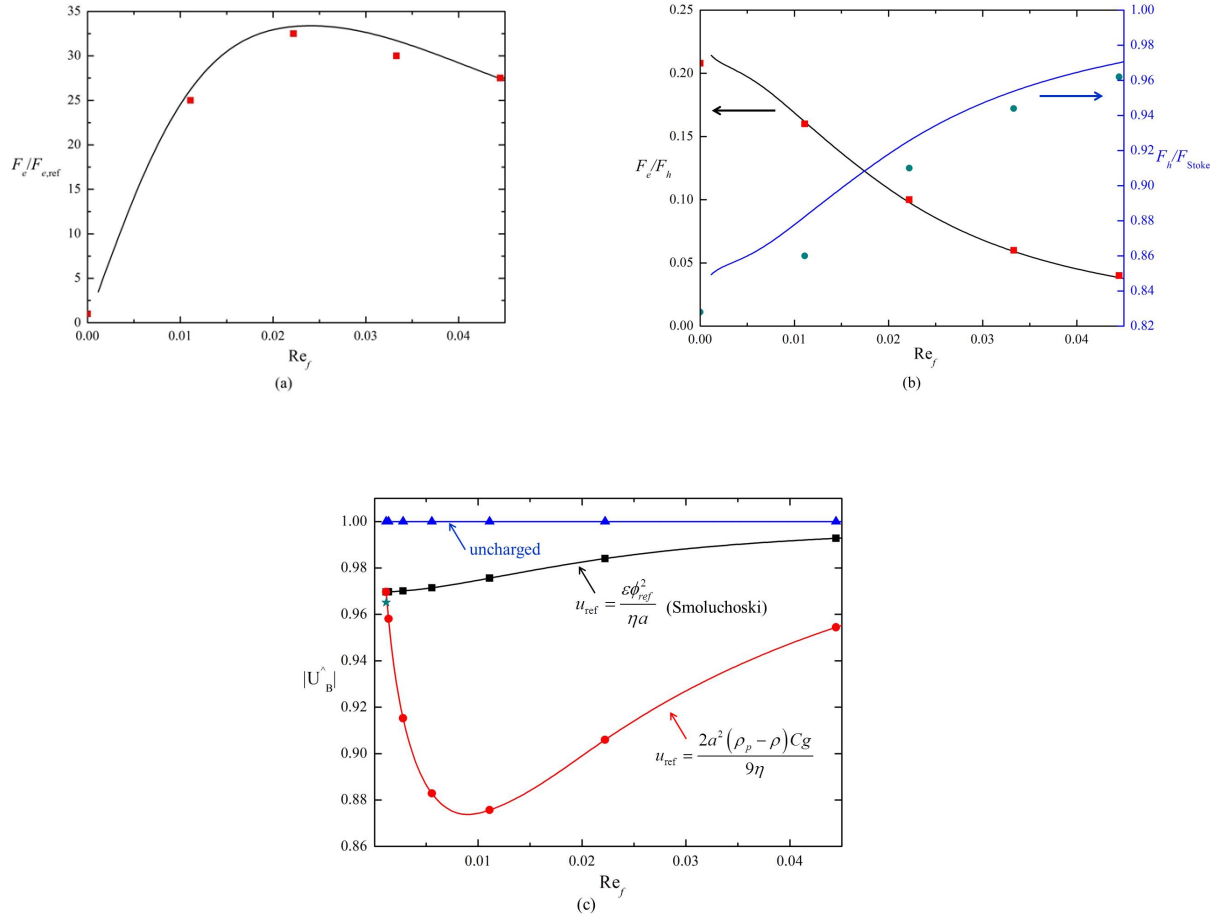


**Fig. S1** Variation of the scaled electric force ( $F_e/F_{e,ref}$ ), (a), ( $F_e/F_h$ ) and ( $F_e/F_{Stokes}$ ), (b), and  $|U_B^hat|$ , (c), with  $Re_f$  for an isolated rigid sphere of radius  $3 \times 10^{-7}$  m, scaled zeta potential  $\zeta = 3$ , and density  $\rho_p = 4000$  kg/m<sup>3</sup> in an aqueous KCl solution at  $\kappa a = 1$ . Discrete symbols: numerical result of Keller et al.;<sup>1</sup> solid curve: present result. The green star symbol in Fig. S1(c) is the analytical result of Keh.<sup>2</sup>

The range of  $Re_f$  considered in Fig. S1(c) is in the creeping flow regime. Therefore, if

$u_{ref} = \epsilon \phi_{ref}^2 / \eta a$  is chosen as the reference velocity, the magnitude of the scaled particle

velocity  $|\hat{U}_B|$  increases with increasing Reynolds number, and  $|\hat{U}_B| \rightarrow 1$  as  $\text{Re}_f \rightarrow 1$ . The blue triangles in Fig. S1(c) denote the sedimentation velocity of a rigid, uncharged sphere (i.e., Stokes' law). Note that the scaled velocity of an uncharged particle remains unity, regardless of the value of  $\text{Re}_f$ . This is because the reference velocity also varies with  $\text{Re}_f$ . The difference between the values of  $|\hat{U}_B|$  represent by dark squares and those by red dots arises from the choice of the reference velocity in the calculation of the hydrodynamic force by eqn (12). As seen in Fig. S1(c), if Smoluchoski velocity is chosen as the reference, then  $|\hat{U}_B|$  increases monotonically with increasing  $\text{Re}_f$ . However, it is interesting to see that if  $u_{\text{ref}} = 2a^2(\rho_p - \rho)Cg/9\eta$  is chosen as the reference velocity,  $|\hat{U}_B|$  shows a local minimum at  $\text{Re}_f \approx 0.1$ , and approaches to unity as  $\text{Re}_f$  gets large. Since the only moving object is the charged particle, the reference velocity should be based on its velocity. Note that although the flow is in the Stokes regime, it is better not to use the Smoluchoski velocity as the reference velocity because the inertial force still plays some role. Therefore,  $u_{\text{ref}} = 2a^2(\rho_p - \rho)Cg/9\eta$  is adopted in the following discussions.

The green star symbol in Fig. S1(c) is the analytical result of Keh and Ding,<sup>2</sup>

$$U = U_0 \left[ 1 - H \frac{\varepsilon \zeta^2}{8\pi\eta} \left( \frac{1}{D_+} + \frac{1}{D_-} \right) + O(\zeta^3) \right], \quad (\text{S1})$$

where  $H = H(\kappa a, \zeta)$  with  $\kappa a$  and  $\zeta$  being the scaled double layer thickness and the scaled zeta potential, respectively. Their result was based on a force balance considering the gravitational, buoyant, electric, and hydrodynamic drag forces acting on a rigid

particle.

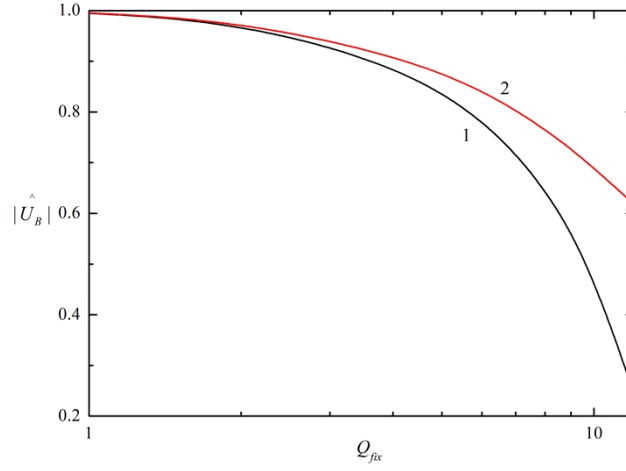


**Fig. S2** Variation of the magnitude of the scaled sedimentation velocity  $|\hat{U}_B|$  with  $Q_{fix}$  for a porous sphere of  $a=500$  nm,  $\rho_p=1700$ ,  $\lambda\bar{a}=1$ , and  $\kappa\bar{a}=1$  with the reference velocity chosen as the electrophoresis velocity in an aqueous KCl solution, corresponding to  $Re_f=1.16\times 10^{-3}$ . Curve 1: analytical result of Keh and Chen<sup>3</sup>; 2: present numerical results.

Our model is furthermore verified by considering the sedimentation of a porous sphere studied analytically by Keh and Chen<sup>3</sup>

$$U = U_0 \left[ 1 - (\kappa a)^4 H Q_{fix}^2 + O(Q_{fix}^3) \right] \quad (S2)$$

$$U_0 = (1 - \varepsilon_p) (\rho_p - \rho) \frac{2a^2 g}{9\eta} \left[ 2(\lambda a) A_1 \alpha(\lambda a) \right] \quad (S3)$$

$U_0$  is the particle velocity for the limiting case of an infinitely dilute suspension of porous spheres,  $A_1 = 3\alpha(\lambda a) + 2(\lambda a)^3 \cosh(\lambda a)$ , and  $\alpha(x) = x \cosh x - \sinh x$ . If  $U_0$  is used as

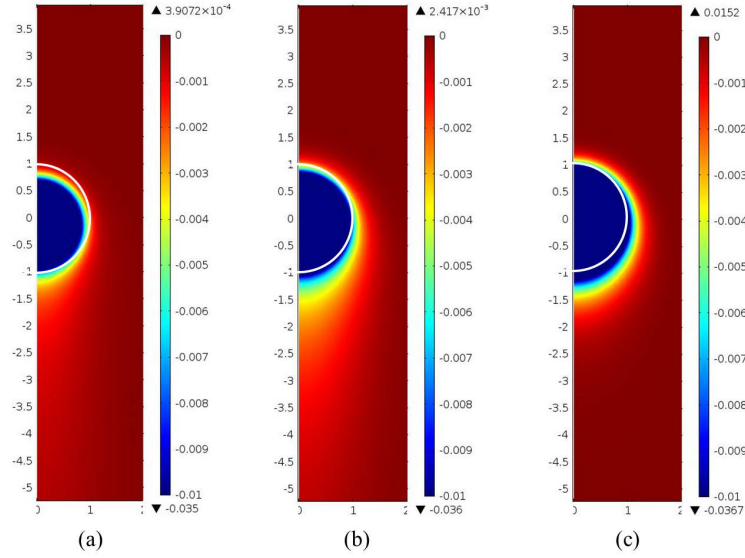
the reference velocity, eqn (S2) becomes

$$|\hat{U}_B| = \left[ 1 - (\kappa a)^4 H Q_{fix}^2 + O(Q_{fix}^3) \right] \quad (S4)$$

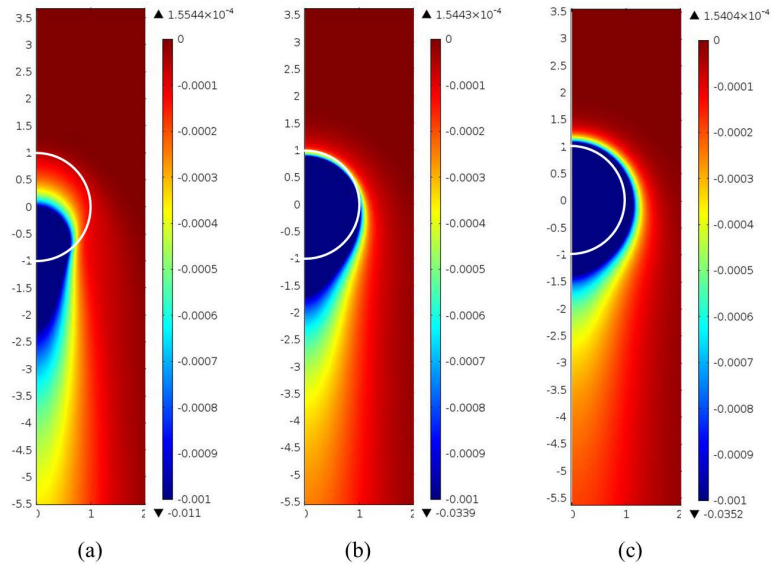
The analysis of Keh and Chen<sup>3</sup> assumed that the system is only slightly distorted from equilibrium, which is valid if  $Q_{fix}$  is sufficiently small. According to eqn (S4), their result is applicable for  $Q_{fix}$  up to second order. Fig. S2 shows that the deviation of their result from the present result becomes serious when  $Q_{fix}$  get large (exceeds ca. 2), as expected.

Table S1. Variations of  $E_{z,avg}^*$  and  $Q_{eff,avg}^*$  for various combinations of  $\bar{\lambda a}$  and  $\bar{\kappa a}$ .

		$\bar{\lambda a}=1$	$\bar{\lambda a}=4$	$\bar{\lambda a}=10$
$\bar{\kappa a}=0.5$	$E_{z,avg}^*$	-0.21603	-0.29471	-0.22146
	$Q_{eff,avg}^*$	0.976574	0.699132	0.581094
$\bar{\kappa a}=0.8$	$E_{z,avg}^*$	-0.53657	-0.53513	-0.3731
	$Q_{eff,avg}^*$	0.916205	0.61466	0.515701



**Fig. S3** Contours of the net ionic concentration ( $C_1-C_2$ ) (mol/m<sup>3</sup>) in the case of Fig. 2(a) on the half plane  $\theta=0$  at  $Q_{fix}=50$ ,  $d/a=0$ ,  $\lambda\bar{a}=4$ , and  $Re_f=0.01$  for three values of  $\kappa\bar{a}$ , 0.8, 2, and 5 in (a), (b), and (c), respectively. White curves denote the particle surface on which the Maxwell stress tensor is integrated to obtain  $F_e^*$ .



**Fig. S4** Contours of the net ionic concentration ( $C_1-C_2$ ) (mol/m<sup>3</sup>) on the half plane  $\theta=0$  at  $Q_{fix}=50$ ,  $d/a=0$ ,  $\kappa\bar{a}=0.5$ , and  $Re_f=0.01$  at three values of  $\lambda\bar{a}$ , 1, 4, and 10 in (a), (b), and (c), respectively. White curves denote the particle surface on which the Maxwell stress tensor is integrated to obtain  $F_e^*$ .

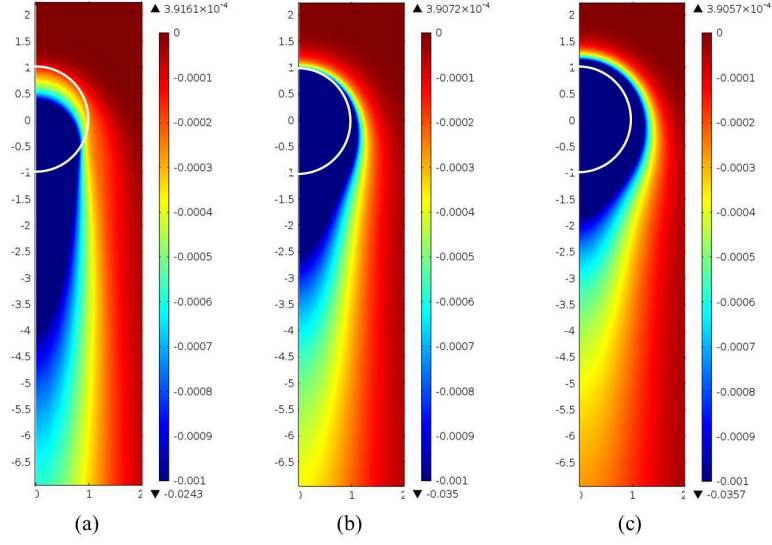


**Fig. S5** Contours of the net ionic concentration ( $C_1-C_2$ ) (mol/m<sup>3</sup>) on the half plane  $\theta=0$  at  $Q_{fix}=50$ ,  $d/a=0$ ,  $\bar{\kappa}a=0.8$ , and  $Re_f=0.01$  at three values of  $\lambda\bar{a}$ , 1, 4, and 10 in (a), (b), and (c), respectively. White curves denote the particle surface on which the Maxwell stress tensor is integrated to obtain  $F_e^*$

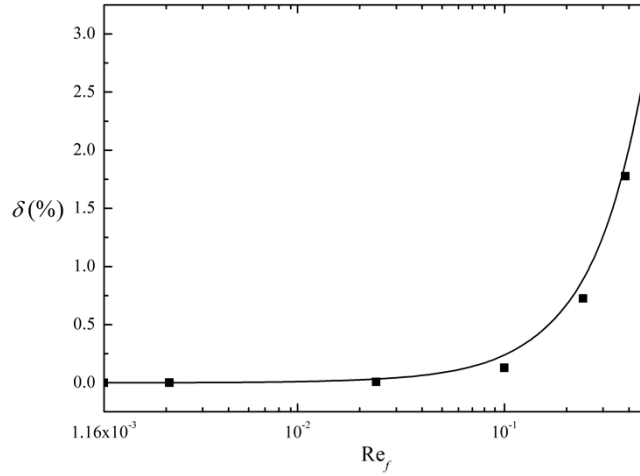


**Fig. S6** Variation of the percentage deviation in the reference hydrodynamic drag  $F_{Stokes} = 6\pi\eta a u_{ref}$  due to neglecting the convective term  $\rho(\mathbf{u} \cdot \nabla \mathbf{u})$  in eqn (4) with  $Re_f$  at  $Q_{fix}=50$ ,  $d/a=0$ , and  $\lambda\bar{a}=4$ .

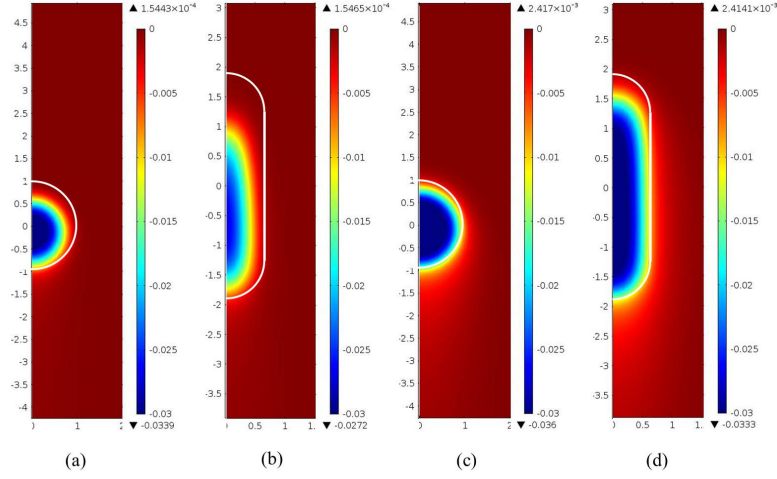


**Fig. S7** Contours of the scaled net ionic concentration ( $C_1-C_2$ ) ( $\text{mol m}^{-3}$ ) on the half plane  $\theta=0$  at  $Q_{fix}=50$ ,  $\lambda\bar{a}=4$ , and  $\text{Re}_f=0.1$  for various combinations of  $(d/a)$  and  $\kappa\bar{a}$ . (a)  $d/a=0$  and  $\kappa\bar{a}=0.5$ , (b)  $d/a=2$  and  $\kappa\bar{a}=0.5$ , (c)  $d/a=0$  and  $\kappa\bar{a}=2$ , (d)  $d/a=2$  and  $\kappa\bar{a}=2$ . White curves denote the particle surface on which the Maxwell stress tensor is integrated to obtain  $F_e^*$

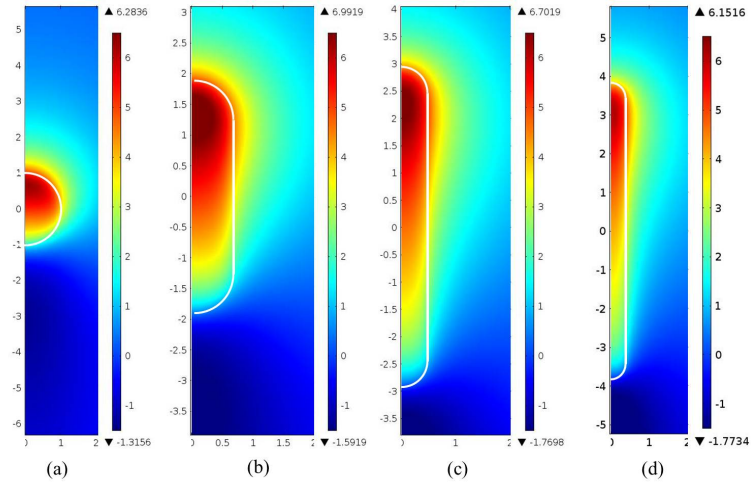


**Fig. S8** Contours of the scaled electric potential,  $\phi^* = \phi/\phi_{ref}$ , on the half plane  $\theta=0$  at  $Q_{fix}=50$ ,  $\lambda\bar{a}=4$ ,  $\kappa\bar{a}=2$ ,  $\lambda\bar{a}=4$ , and  $\text{Re}_f=0.1$ , for various values of  $(d/a)$ , 0, 2, 5, and 8 in (a), (b), (c), and (d), respectively. White curves denote the particle surface on which the Maxwell stress tensor is integrated to obtain  $F_e^*$ .

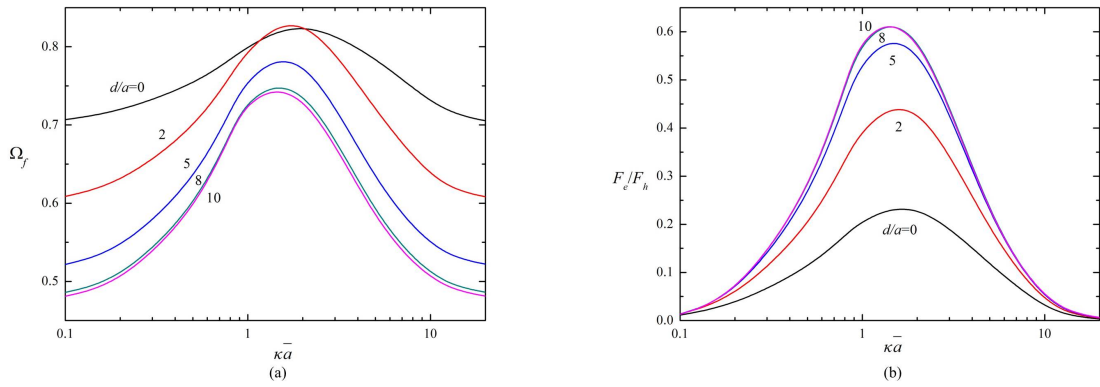


**Fig. S9** Variation of the drag factor  $\Omega_f$ , (a), and  $(F_e/F_h)$ , (b), with  $\bar{\kappa a}$  for various values of PE aspect ratio ( $d/a$ ) at  $Q_{fix}=50$ ,  $\bar{\lambda a}=4$ , and  $Re_f=0.01$ .

## References

1. F. Keller, M. Feist, H. Nirschl and W. Dörfler, *Journal of Colloid and Interface Science*, 2010, **344**, 228-236.
2. H. J. Keh and J. M. Ding, *Journal of Colloid and Interface Science*, 2000, **227**, 540-552.
3. H. J. Keh and W. C. Chen, *Journal of Colloid and Interface Science*, 2006, **296**, 710-720.